

A Study of the Azimuthal Electron Drift in an $E \times B$ Discharge Using a Non-invasive Antenna Array

Cliff A. Thomas, Nicolas Gascon, and Mark A. Cappelli
Mechanical Engineering Department
Stanford University, Stanford CA 94305-3032

A non-invasive antenna array is used to study medium and high-frequency plasma instabilities and to generate a spatial and temporal map of the azimuthal drift current in a coaxial Hall discharge. Typical Hall plasmas are characterized by strongly magnetized electrons and streaming ions and it is hoped that a better understanding of the azimuthal drift in such devices might further elucidate the importance of various mechanisms on bulk electron mobility in the broader range of $E \times B$ discharge plasmas. In this study, the time dependent measurements of induced current in loop antennas encircling the outer insulating channel walls during quasi-steady state are used to qualitatively investigate the correlation of instabilities with fluctuations in electron mobility. The calibration of the antenna array is done numerically and verified experimentally at multiple frequencies. High frequency oscillations consistent with those described in the previous literature are reported. In addition, preliminary results of using the array to characterize the azimuthal current distribution are obtained using fast current interruption on a timescale shorter than that characterizing plasma relaxation.

I. INTRODUCTION

The use of a loop antenna external to the outer dielectric wall for the non-invasive investigation of the azimuthal electron drift in an $E \times B$ discharge is a diagnostic whose initial development dates to the mid 1970's and perhaps even earlier [1, 2]. In these prior studies, it was implemented to estimate the total azimuthal drift current and its 'center of gravity' in a coaxial discharge [1, 2]. These measurements have been validated to a significant degree by complementary antenna measurements [3], 1-D and 2-D numerical codes, and a host of more invasive probing techniques [4]. The use of the loop antenna is predicated upon several simple notions: (i) that the loop antenna is an excellent indicator for local oscillating magnetic dipoles of antenna-comparable spatial geometry (especially if the antenna and dipole are co-linear); (ii) that the bandwidth of the loop antenna's response is large (and easily predicted for a wide variety of boundary conditions); (iii) that the antenna is easily fabricated and can provide considerable gain, and (iv) that the geometry of the coaxial discharge is easily lent to a axially symmetric treatment favorably matched by practical constraints on loop antenna design, implementation, and analysis.

A loop antenna array is a natural extension of

this line of reasoning given that the response of any particular antenna is dependent on the orientation and precise location of any neighboring transmitting magnetic dipoles. Under the constraints that the receiving and transmitting components are collinear the problem of determining the spatial location and magnitude of a finite (or continuous) distribution of oscillating dipoles is considerably simplified. Given that the azimuthal perturbations in the drift current are expected to be negligible with respect to the total drift at any given location, the drift current is considered to generate a finite dimension magnetic dipole that can be investigated with a suitably chosen antenna array.

II. EXPERIMENTAL SETUP

II.1. Stanford Hall Thruster (SHT)

The $E \times B$ plasma discharge used in this study is a laboratory version of a low-power Hall thruster (<1 kW), details regarding which can be found in existing previous publications [5, 6]. The source consists of an annular alumina channel 90mm in diameter, 11mm in width, and 80mm in length. The magnetic circuit consists of four outer coils, one inner coil, and three iron plates providing a radial magnetic field whose peak is 5mm upstream of the exit plane. Details regarding the magnetic circuit are also available in a previous paper [7]. A hollow stainless steel ring with 32 holes 0.5mm in diameter serves as the anode and propellant feed. A commercially available hollow cathode (Ion Tech HCN-252) neutralizes the discharge.

II.2. Vacuum Chamber

The experiments reported here were performed in a 3.25-m long stainless steel vacuum chamber 1.25-m in diameter with a pressure of 10^{-5} mbar (as measured using an uncorrected ion gauge) during nominal operation of the thruster. This was accomplished using two CVI cryogenic pumps (model number CGR-511 LS) with accompanying liquid nitrogen shrouds. Separate DC power supplies were used to power the discharge, cathode keeper, cathode heater, and electromagnetic coils. The cathode was kept at tank potential (ground). Measurements of the discharge current were made using a powered differential amplifier (Tektronix P5200) placed across a 4Ω load in series with the discharge. Measurements of the antenna response were captured using two digital oscilloscopes that could be simultaneously triggered from a signal proportional to the discharge current (a Tektronix TDS 3014 and a Tektronix TDS 3054).

II.3. Fast Switch

In order to accomplish fast current interruption a manually controlled power MOSFET was placed in series with the discharge (see Fig. 1). It was controlled using floating CMOS logic components and triggered by a simple mechanical switch. In this manner current commutation in 100-200 ns was achieved.

II.4. Antenna Array

To precisely align and maintain the position of several antennae with respect to the SHT, six tracks were cut in a Teflon sleeve sized to just clear the outer diameter of the ceramic wall. The spacing of the tracks was 1.6 mm, and they were sized to secure 0.5 mm diameter insulated wire. With the wire antennae in place (and each connected to a matching 50Ω cable with BNC termination) the entire

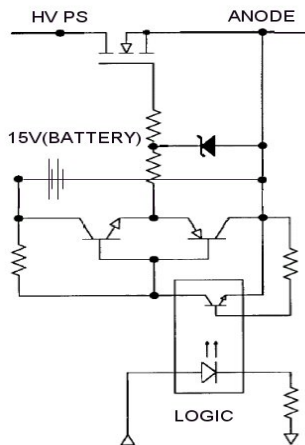


Figure 1. Schematic of fast current interruption circuit.

assembly was thinly coated with BN to help resist the chamber environment. One end of the antenna array was polished to that it could be repeatedly positioned next to the magnetic pole piece at the exit plane (by abutting it) with as little error as possible. Surface interference was measured to be ~ 0.2 mm, and this was included in all relevant computations. Pictures of the final antenna assembly (as mounted to the SHT) and a diagram of the antenna placement with respect to the SHT follows in Figs. 2 and 3.

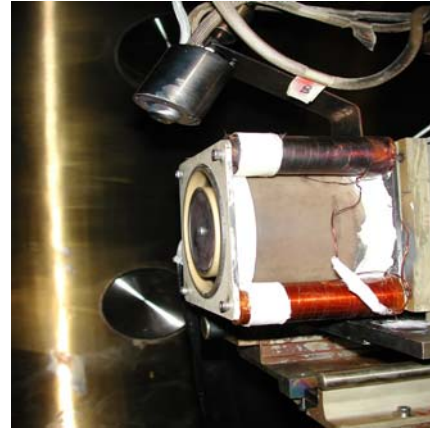


Figure 2. The antenna assembly appears as a white ring abutting the magnetic pole piece on the SHT.

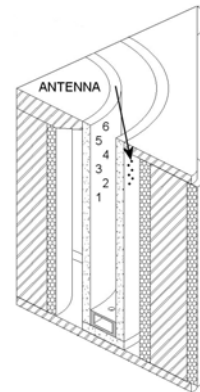


Figure 3. Diagram of antenna array location and numbering scheme.

III. AZIMUTHAL DRIFT DIAGNOSTIC

III.1. Problem Formulation

Determining the azimuthal drift from the antenna array's temporal response requires an inverse solution to Maxwell's field equations. To solve for the voltage induced in a pickup coil, Maxwell's equations must be satisfied for boundary conditions consistent with the metal and ceramic containment of the plasma discharge. The forward problem is

particularly troublesome - the inverse one is more so, but both are made considerably easier by taking advantage of symmetry and several simple approximations.

Faraday's Law of induction can be written utilizing the radial symmetry of the coaxial discharge and Stokes' Theorem (assuming that transients are of a timescale that a voltage, V , induced in an external coil can be properly defined for the relevant length scale) to provide an integral formula more readily related to the experimentally measured antenna response, i.e.,

$$V = -\frac{\partial}{\partial t} \oiint (H + M) \cdot \hat{n} dA \quad (1)$$

Here, H is the magnetic field strength, and M is the magnetization of the medium, which must be determined by the full solution of Maxwell's equations. In its most basic form, Eqn. 1 can be represented by a Green's function solution, fully consistent with all problem constraints, to the azimuthal drift current in frequency space, with the contribution δV_ω to the total voltage V in the coil located at \vec{x} arising from a line current density J_θ at position \vec{x}' , expressed as:

$$\delta V_\omega(\vec{x}) = -G_\omega(\vec{x}, \vec{x}') \left[\frac{\partial J_\theta(\vec{x}', t)}{\partial t} \right]_\omega \delta A(\vec{x}') \quad (2)$$

Here, $\delta A(\vec{x}')$ is a differential area element normal to the azimuthal direction at the axial position \vec{x}' , and G_ω is the associated Green's function. Eqn. 2 is the preferred launching point for the inverse problem, as the unknown current density can be approximated to a specifiable set of functional parameters dependent mainly on the accuracy of the voltage measurement and the precision of the antenna registration. The forward and reverse problem herein considered depends on the strict applicability of frequency superposition as described in Eqn. 2 – an equation for

which non-linearity can arise due to the variable magnetic permeability of iron (which is a primary component in the magnetic circuit). Fortunately, the Hall current causes only minor perturbations in the magnetization of the poles, and so changes in the effective permeability due to mode interaction is expected to be negligible.

III.2. Special Considerations

It is important to note that the experimentally measured voltage will also depend on the self-inductance of the pickup coil. If ϕ is the voltage induced across a small but finite air gap in the antenna's length due to a change in area-integrated flux the measured voltage must be corrected by:

$$\phi_\omega = (i\omega L_\omega + Z_\omega) I_\omega \quad (3)$$

Here, Z_ω is the oscilloscope impedance (usually 50Ω), I_ω is the loop current, and L_ω is the impedance of the loop antenna. Fortunately, for most frequencies the self-inductance is small, and at high frequencies the effective self-inductance is reduced below expected levels due to shielding by neighboring conducting surfaces (the pole pieces). For the purposes of this study it was found that the antennas' self-inductances were negligible (as verified by experimental measurement and numerical calculation), and at frequencies of 50MHz a correction of only 2% was necessary. At higher frequencies the error quickly grew – thus, the extension of the infinite frequency analysis above 50MHz is purposely avoided.

It is noteworthy that the computation of the Green's function is fairly laborious, but must be done precisely to ensure accuracy in the inverse solution to Eqn. 2. Repeatedly in the previous literature the Green's function solution is approximated by experiment [1-3]. A metal loop is placed inside the boundary of interest and a current in this loop is either sinusoidally excited in time, or it is excited

COIL:		1	2	3	4	5	6
$ G/\omega $		10^8 V-s/A	10^8 V-s/A	10^8 V-s/A	10^8 V-s/A	10^8 V-s/A	10^8 V-s/A
10 kHz	Numerical	4.01	4.51	3.89	4.23	3.68	3.87
10 kHz	Experimental	3.90	4.43	3.90	4.22	3.80	4.01
10 MHz	Numerical	0.38	0.84	0.74	1.15	9.43	1.23
10 MHz	Experimental	0.42	0.84	0.76	1.14	9.25	1.25

Table 1. The results of the numerical model versus calibration figures at 10 kHz and 10 MHz for a small coil centered in the discharge channel at the exit plane. Errors in both sets of data are of order 10% or less.

and/or interrupted on a timescale characteristic of the phenomena that the antenna is intended to study. In this way a rough approximation of G_ω for a given spatial position can be found. This procedure is also used here. However, unlike previous studies, a detailed finite element model is used to numerically determine the frequency dependent Green's function for a multitude of antenna/calibration coil spatial permutations. This was done for two reasons: (i) to more accurately capture differences in G_ω due to small changes in spatial location, and (ii) the *metal* calibration coil itself changes the boundary conditions and at high frequencies its current is rather narrowly confined to its surface (a condition rather different than the homogenous distribution generally assumed for calibration purposes).

The numerical approach to the Green's function calculation is not presented in detail here, but a comparison is made between experiment and numerical calculation at two disparate frequencies (see Table I). In general the level of agreement is within a few percent - a number well within the experimental error of the calibration tests.

It is further noteworthy that the presence of the discharge plasma in the actual experiment is assumed to have a negligible impact on the calculations - i.e., the quasineutral Xe plasma is the working medium and for frequencies of interest has no appreciable magnetic qualities. Furthermore, though the Xe plasma frequency is much greater than the range of electromagnetic frequencies investigated, the plasma is sufficiently collisional as to make the effective skin depth far greater than the plasma dimensions. Thus, the Xe is assumed to behave as free space in all numerical computations.

III.3. Fast Current Interruption

To determine the azimuthal drift current and its distribution within the channel, the discharge current is commutated on a timescale significantly shorter than the expected plasma relaxation time. As addressed in the next section, the commutation circuit is designed to eliminate the axial electric field (and the azimuthal drift) on a timescale of 100-200 ns. This is significantly shorter than the fastest avenue for electron energy or population loss, including collisional - radiative processes, wall collision/neutralization, and ionization processes. For example, the electron loss rate due to recombination at the wall can be approximated by considering the time it would take an electron to cross the channel radially, but this is limited by space-charge effects coupled to the ion mass, and so, is not as fast a process as might be anticipated. The characteristic decay time is then found by considering the Bohm flux to be:

$$\tau = \frac{\Delta R}{1.2 \sqrt{kT_e / M_i}}. \quad (4)$$

Here, ΔR is the channel width, T_e is the electron temperature, and M_i is the ion mass. For $\Delta R = 12$ mm and for a mean electron energy of 10eV, τ is estimated to be 3700 ns. Of course, the expected relaxation time is shorter than this due to the combined influence of *all* relevant relaxation processes, but not considerably so. Line-of-sight emission measurements on Hall discharges under similar conditions indicate relaxation times of order 1000 ns [3]. As a result, the plasma density is frozen while the azimuthal drift is brought to zero *coherently* across the channel with the anode potential. The antenna response can then be used to study the state of the azimuthal drift at the moment of discharge disruption, and the fact that the azimuthal drift *must* decay to zero serves as a useful temporal boundary condition. By performing repeated tests the average azimuthal drift can be calculated, and an envelope enclosing its maximum large-scale perturbations can be found.

The spatial distribution of the drift is found by taking multiple antennas (in this case, six) at different locations, and by calculating the infinite time frequency content of their temporal response during a current interruption event. A single parameterized function of space and time is fit to Eqn. 2 with the least possible error. In all following computations a five-parameter fit to the spatial distribution for the current density, consisting of a double-Gaussian of unknown center and half-width in two separate dimensions (radial and axial), is taken. This approach is chosen because it is consistent with the expected drift profile and, upon analysis, provided the best fit of the functional spaces investigated.

Since fast current interruption effectively enforces the coherent decay of the azimuthal drift across the channel a simple decomposition of the current density is possible, i.e.,

$$J_\theta = I_\theta X(\vec{x}') T(t) \quad (5)$$

Here, T is most generally a function of time and space ranging from zero to one, but in this instance is restricted to time. X is the aforementioned double Gaussian, but normalized such that the integration of J_θ across the channel for $T = 1$ yields the total azimuthal drift current. Substitution of Eqn. 5 into Eqn. 2 yields:

$$\delta V_\omega(\vec{x}) = -I_\theta G_\omega(\vec{x}, \vec{x}') X(\vec{x}') \left[\frac{\partial T}{\partial t} \right]_\omega \delta A(x'). \quad (6)$$

Since $I_\theta \left[\frac{\partial T}{\partial t} \right]_\omega$ is independent of coil location it is calculated as a function of frequency with an appropriate guess at X by:

$$I_\theta \left[\frac{\partial T}{\partial t} \right]_\omega = \frac{\sum_{\vec{x}} -V_\omega(\vec{x})}{\sum_{\vec{x}} \int_{\vec{x}'} G_\omega(\vec{x}, \vec{x}') X(\vec{x}') \delta A(x')}. \quad (7)$$

Iteration on X is accomplished given the result of the above by considering frequencies with mathematically substantial signal integrity (those frequencies whose response significantly exceeds the overlying noise - this is characteristic of the frequency band signifying the main temporal decay). The parameters of X are adjusted slightly to reduce the norm of the residual :

$$\rho_\omega^i = V_\omega^i + I \left[\frac{\partial T}{\partial t} \right]_\omega \int_{\vec{x}'} G_\omega^i(\vec{x}') X(\vec{x}') dA(x') \quad (8)$$

as given by the equation for the i^{th} antenna at a given frequency within the band of relevant frequency response. Note that the components for any given residual are not normalized; as weight should be assigned to those components of any given residual that are inherently larger. Thus, component weighting is proportional to variable magnitude. This process is repeated until convergence is achieved alongside a parallel algorithm ensuring solutions that approach zero as time proceeds to infinity.

III.4. Dynamic Current Oscillation

For the setup considered herein a direct space/time analysis of low frequency perturbations (such as the breathing mode) was impossible, as the current antenna array and measurement system does not provide enough gain to produce signals substantially above the system noise at such low frequencies. Regardless, the magnitude and distribution of perturbations to the average azimuthal drift can be understood by considering the range of solutions garnered via fast current interruption, since any single solution can be considered to be a snapshot in the normal operational envelope.

Information pertaining to high and low frequency instabilities in the azimuthal drift and their possible correlation to fluctuations in the electron mobility is available by virtue of a finite-time frequency analysis of representative steady state oscillatory periods. For these measurements data is taken of the output of antennas 1, 2, 4, and 5, concurrent with a measurement of the discharge current. These tests are limited in duration to 10^4 points by the Tektronix oscilloscopes in use, but could be made with a minimum Δt of 2 ns. As a result exceptionally high frequency perturbations could be investigated, but the range of results presented herein is 10kHz to 20MHz.

IV. EXPERIMENTAL RESULTS

IV.1. Fast Current Interruption

Several tests were carried out with the anode potential at 180V. The average discharge current was 1.51A and the magnet current was 200mA. Fast current interruption proceeded as expected except for some overshoot/ringing in the anode potential that was unanticipated. Since this phenomena manifested itself over timescales similar to the plasma relaxation time (and the plasma is not expected to relax in a consistent manner across the channel) some additional error was introduced, but is not expected to significantly impact the calculation. An example plot of the anode potential is provided in Fig. 4.

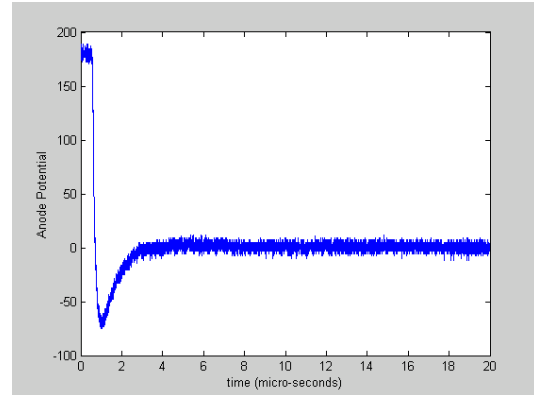


Figure 4. Anode Potential vs time during fast current interruption.

A typical trace of the antenna voltage for a commutation event is shown in Fig. 5. below for antennas 1-6. Antenna location has an obvious impact on the recorded signal.

The current density distribution was calculated for each test as earlier explained, and a representative result follows in Fig. 6. The current density is seen to

peak near the pole piece adjacent the exit plane (close to the region of maximum magnetic field) and is preferentially weighted towards the inner electromagnetic pole (in agreement with previous reports as presented in [1,2,4]). The result also appears consistent with the axial location of the azimuthal current extracted from detailed plasma property measurements [10]. The total azimuthal drift current for this case is 24 A.

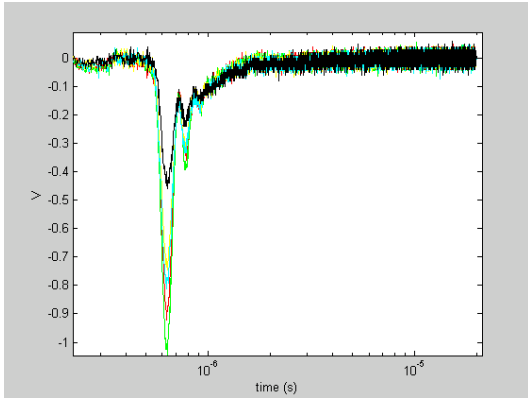


Figure 5. Typical trace of antenna response during fast current interruption.

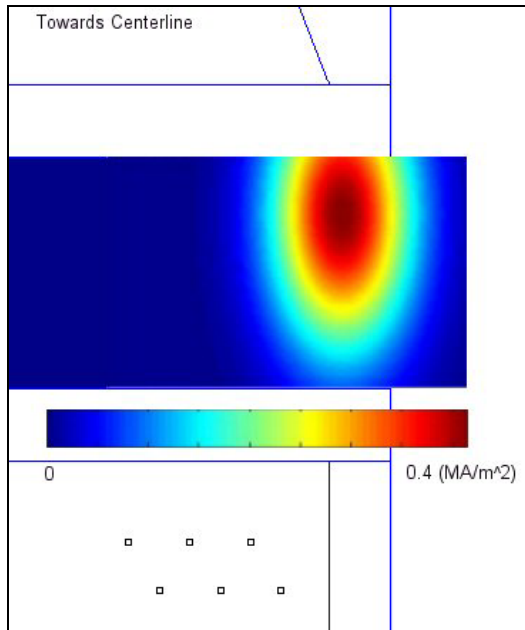


Figure 6. 2-D map of Azimuthal Drift at 180V anode potential, 200mA magnet current, and 1.51A discharge current. For use as a length scale, the height of the domain is 12 mm, i.e., the width of the discharge channel.

A plot of the radially-averaged current density versus axial position, and its comparison to the distribution in the radial magnetic field strength is provided in Fig. 7. Again, it is apparent that the peak in the magnetic field appears close to the maximum current density, though there is an offset of 1-2 mm. It should be noted also that the half-width of the current density profile is significantly shorter than that of the radial magnetic field.

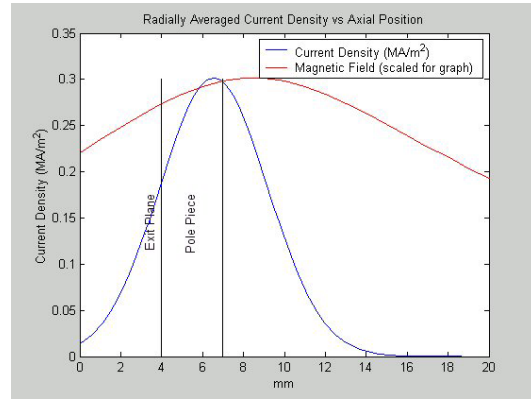


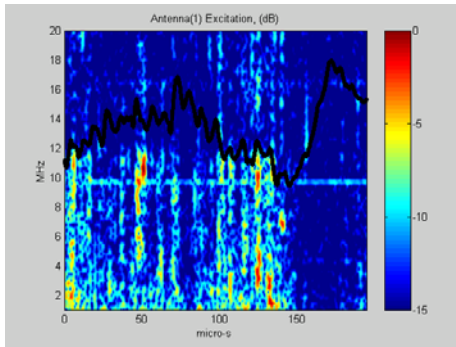
Figure 7. Comparison of the axial variation in the current density to the magnetic field. Also shown for comparison is the location of the exit plane and the center of the pole piece.

It is estimated that the magnitude of the total azimuthal drift current is accurate to approximately 10%, and the position of the maximum drift is accurate to ~ 1 mm.

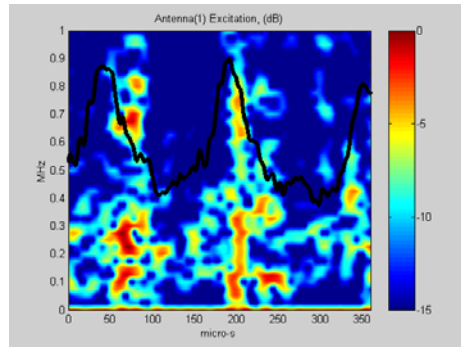
IV.2. Dynamic Current Oscillation

As earlier described, measurements of the antenna voltage response were analyzed for their frequency content as a function of time. Typical results of temporally-sliding spectral maps and discharge current for a range of discharge voltage are shown in Fig. 8. The results for the analysis of antennas 2, 4, and 5 are not shown since they are qualitatively similar. The timescales of measurement were chosen to allow signal analysis over a wide frequency band, yet still resolve temporal variations in the frequency content consistent with fluctuations in the discharge current.

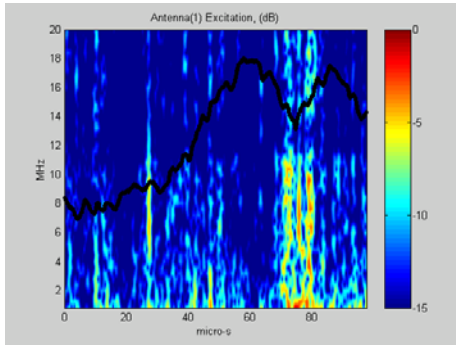
A rich spectrum of disturbances is seen ranging from a few 10's of kHz to 10's of MHz, with a variety of disturbances at frequencies where there are expected instabilities (as reported in [8, 9]). Most striking though is the obvious correlation between instabilities and fluctuations in the discharge current as previously evidenced by [3, 10]. Instabilities occur in conjunction with fluctuations in the discharge, and are noticeably decreased (or even



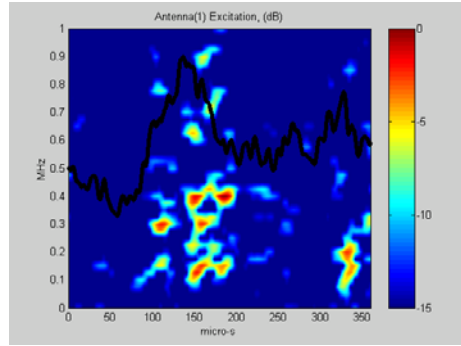
(a) – 100 V, 1.55 A, 125 mA



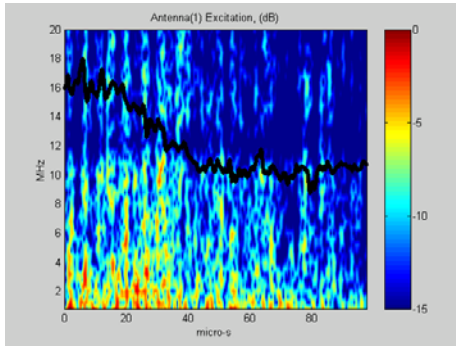
(b) – 100V, 1.55 A, 125 mA (expanded scale)



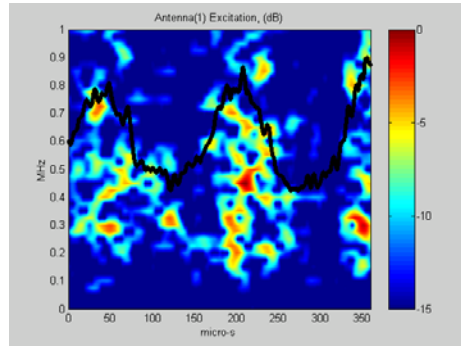
(c) – 110 V, 1.26 A, 200 mA



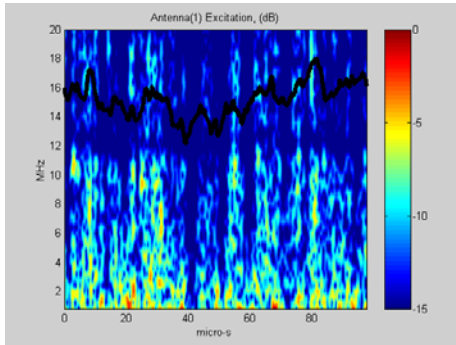
(d) – 110 V, 1.26 A, 200 mA (expanded scale)



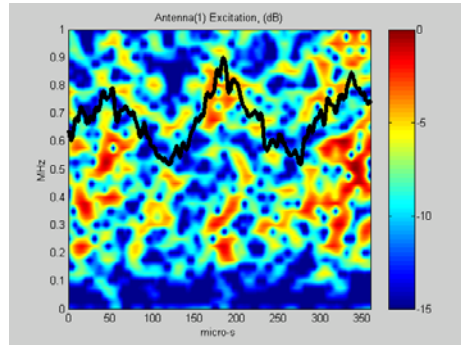
(e) 160 V, 1.50 A, 200 mA



(f) – 160 V, 1.50 A, 200 mA (expanded scale)



(g) – 180 V, 1.68 A, 200 mA



(h) – 180 V, 1.68 A, 200 mA (expanded scale)

Figure 8. Spectral maps of the antenna voltage as a function of time. Also superimposed is the discharge current (black line). Operating parameters listed refer to (i) discharge voltage, (ii) discharge current, and (iii) magnet current.

absent) when the discharge is monotonically increasing. The timescales of the disturbances are remarkably consistent with the period of change in the discharge, and imply a relation between instabilities across many frequency scales and the cross-field electron mobility (as considered by [11]). Furthermore, the results are consistent with expectations that high frequency disturbances in the range of a few MHz should generally be short lived and that low frequency disturbances (consistent with azimuthal waves, the ionization instability, etc.) would manifest themselves over longer timescales. Finally, it appears that an increase in the magnetic field (achieved by increasing current through the magnetic circuit) appears to dampen a variety of instabilities, as seen by comparing Figs. 8(b) and 8(d).

V. SUMMARY

Fast current interruption and external detection of plasma currents using surrounding antenna array - a novel non-invasive method for investigating the azimuthal drift in a Hall thruster - is examined as a diagnostic tool, and preliminary results are presented and found to be consistent with existing literature and theoretical expectations.

The antenna array is also used to capture quasi steady-state data during normal thruster operation and provides insight into the relationship between medium and high frequency instabilities and variations in the cross-field electron mobility. As witnessed in previous studies a strong correlation between instabilities and strong reductions in the discharge current is evident.

Future research is planned, to further investigate instabilities and their relationship with quasi steady-state operation. The magnitude and location of the average azimuthal drift at a variety of discharge parameters will also be investigated and compared to the prediction of numerical models.

Acknowledgements

Funding for this research was provided by the Air Force Office of Scientific Research. N. Gascon was supported by a fellowship from the European Space Agency. C. Thomas received support from the National Science Foundation, and from Stanford University through the SGF Fellowship Program.

References

[1] V.N. Dem'yanenko, I.P. Zubkov, S.V. Lebedev, and A.I. Morozov, "Induction method for measuring the azimuthal drift current in a Hall-

current accelerator", *Sov. Phys. Tech. Phys.* 23(3), pp. 376-377, March 1978.

- [2] A.I. Bugrova, V.S. Versotskii, and V.K. Kharchevnikov, "Determination of the radial center of gravity of an azimuthal drift current in accelerators with closed electron drift", *Sov. Phys. Tech. Phys.* 25(10), pp. 1307-1308, October 1980.
- [3] Mathieu Prioul, André Bouchoule, et al., "Insights on the physics of Hall thrusters through fast current interruptions and discharge transients", 27th International Electric Propulsion Conference, IEPC-01-059.
- [4] A.I. Bugrova, A.I. Morozov, and V.K. Kharchevnikov, "Probe measurements of drift current in a Hall accelerator", *Sov. Phys. Tech. Phys.* 30(6), pp. 610-612, June 1985.
- [5] N.B. Meezan, W.A. Hargus, and M.A. Cappelli, "Optical and electrostatic characterization of oscillatory Hall discharge behavior", AIAA-98-3502, 34th Joint Propulsion Conference, Cleveland, OH, July 1998.
- [6] W.A. Hargus and M.A. Cappelli, "Laser induced fluorescence measurements on a laboratory Hall thruster", AIAA Paper No. 98-3645, 34th Joint Propulsion Conference, Cleveland, OH, July 1998.
- [7] W.A. Hargus, "Investigation of the plasma acceleration mechanism within a co-axial Hall thruster", Ph.D. Thesis, Mechanical Engineering Department, Stanford University, 2001.
- [8] E.Y. Choueiri, "Plasma oscillations in Hall thrusters", *Physics of Plasmas*, Vol. 8 Num. 4, April 2001.
- [9] A. Lazurenko, V. Vial, A. Bouchoule, et al, "Characterization of microinstabilities in a Hall thruster plasma: experimental and PIC code simulation results, physical interpretation and impact on transverse electron transport", 29th International Electric Propulsion Conference, IEPC-2018.
- [10] Nathan B. Meezan, William A. Hargus Jr., and Mark Cappelli, "Anomalous electron mobility in a coaxial Hall discharge plasma", *Physical Review E*, Vol. 63, 026410.
- [11] Yu. V. Esipchuk and G.N. Tilinin, "Drift instability in a Hall-current plasma accelerator", *Sov. Phys. Tech. Phys.* 21(4), pp. 417-423, April 1976.